ANTEC® 2020 PAPERS

ANTEC® 2020: THE VIRTUAL EDITION

ENHANCEMENT OF BINDING MATRIX STIFFNESS IN COMPOSITE FILAMENT CO-EXTRUSION ADDITIVE MANUFACTURING

Chethan Savandaiah[1, 3], *Julia Maurer*[2], *Juergen Lesslhumer*[1], *Andreas Haider*[1], *Georg Steinbichler*[3]

[1]*Kompetenzzentrum Holz GmbH, Linz, Austria*

[2]*Research Group Computed Tomography, University of Applied Sciences Upper Austria, Wels, Austria*

[3]*Institute of Polymer Injection Molding and Process Automation, Johannes Kepler University, Linz, Austria*

Abstract

The Flexural modulus and strength are an intrinsic aspect of parts produced via dual matrix composite filament co-extrusion (CFC) based additive manufacturing. In this research work, the main objective is to optimize thermoplastic's (TP) flexural properties by reinforcing it with particulate fillers for CFC printed parts. Accordingly, an effort has been made in this respect and neat Polyamide-6 (PA6) and its composite (PA6.CF) was chosen as a binding matrix for CFC flexural specimens. The PA6 binding matrix is reinforced with particulate carbon fibers (PCF). To improve the compatibility between the PCF and matrix, stearyl titanate coupling agent (1.5 wt. %) was utilized. Constraints such as defects and porosity are of critical attributes and play a vital role in defining the mechanical performance of the 3D printed parts. Herein, the printed specimens were subjected to a non-destructive testing method: micro-computed thermography (µ-CT). PA6 and reinforced PA6 specimen revealed similar porosity and defect volume. Furthermore, the three-point bending test results of 3D printed CFC composite with PA6.CF as a binding matrix showed approx. 46% increase in flexural stiffness and 27% increase in flexural strength when compared to CFC specimens printed with neat PA6 as a binding matrix. In addition, the cryo-fractured fractography of carbon composite filament, an epoxy-based thermo-cured continuous carbon fiber, revealed even distribution of carbon fibers with no visible voids.

Introduction

Recently, the increase in demand for lightweight design approaches in aerospace and automotive industries has enabled a paradigm shift towards low-cost manufacturing processes for high performance continuous fiber-reinforced polymers (CFRP). This outlook has prompted several additive manufacturing (AM) approach to exploit the synergy of 2.5 degrees of freedom (3D printing) or multi-axis robot arm combined with continuous fiber printing head that enables the fiber steering concept to fabricate the state of the art composite lightweight parts.

In continuous fiber-reinforced thermoplastic (CFRTP) AM, Tian et al. [1] and Li et al. [2] studied the influence of processing parameters on mechanical properties. Meng et al. [3] investigated interlaminar delamination between continuous carbon fiber and technical polymer polyetheretherketone (PEEK) and studied its rheological effects on impregnation. Werken et al. [4] did extensive study on porosity, process parameters and its influence on mechanical performance composites and performed FE analysis validation for fiber layup. Peng et al. [5] investigated the influence of combining short and continuous carbon fiber on mechanical properties and reported the combinations outperformed neat filament and improved strength significantly. Eichenhofer et al. [6] investigated the approach of multi-axis robotic arm for highly anisotropic fiber layup to produce ultra-lightweight lattice structure and reported the outstanding stiffness-strength to density performance.

In newly developed dual matrix CFC AM, Andrey et al. detailed the process, design, mechanical characterization and the finite elemental analysis (FEA) for lightweight lattice structured small drone [7]. The authors also investigated the mechanical properties of PLA reinforced with CCF fibers. Similarly, Adumitroaie et al. [8] well- articulates the benefits of fabrication via dual matrix CFC technology. The dual matrices CFC AM is analogous to the coating process in pressure-type die, where the processes involve binding of the carbon composite filament (CCF) with a TP, reinforced and un-reinforced alike, inside the melting chamber (see Figure 1) [9]. The CCF is carbon fibers (1.5k) pre-cured with a thermoset resin, a patented material developed by Anisoprint [10].

There are two main reasons for the use of complex material combinations in dual matrices CFC. Firstly, a low viscous, heat-cured resin such as epoxy is well suited for dry fiber wetting and realizes efficient, flawless processing of fiber impregnation for the production of high strength CCF. On the contrary, high viscous TP for dry fiber impregnation leads to a poor wettability and defects and also restricts the areas of application.

Secondly, TP filaments are widely used and have well-established process parameters for fused filament fabrication (FFF) type 3D printers. This enables to use and modify various engineering TP matrices such as reinforced PA6, PEEK, PEI et cetera. as a binding material and exploit the synergy by combining TP (reinforced and unreinforced) and CCF for the high-performance thermo-mechanical application.

It's a known fact that the strength of carbon fibers lies along its axis and lacks along its transversal axis and the same is molded into CCF. Thus, the load bearing ability in the transversal axis is transferred to the polymer matrix. Several articles details improving the modulus and mechanical strength of TP's by successfully modifying and reinforcing it with fillers (mineral, glass spheres) [11, 12] and fibers (particulate, short and long fibers). Especially, carbon fiber reinforced TP's for 3D printing showed highly anisotropic properties such as high heat deflection temperature, increased modulus, increased part strength along the fiber orientation and more importantly high dimensional accuracy [13, 14] (see Figure 2).

This article gives an insight into the development of different matrices, subsequent processing and its effect on the flexural performance of the 3D printed parts via newly developed CFC 3D printer. Furthermore, CFC technology is relatively new, the optimized materials and its parametric data are not readily available for high thermo-mechanical applications. This article will help the CFC technology users to identify and select TP binding matrix according to the end-user application.

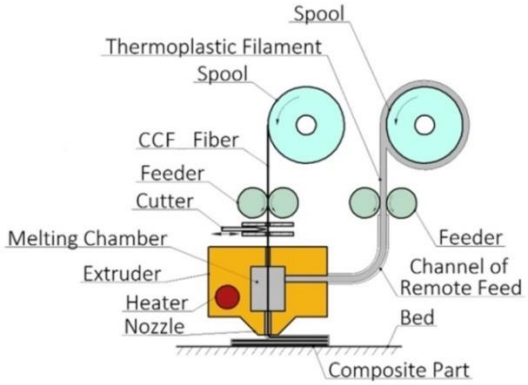

Figure 1 Graphical representation of the printing process of CFC print head [7]

Materials and Methods

Film extrusion grade PA6 (density 1.130 g/cm^3 and melting temperature 220-225 °C) was purchased from DSM, Austria. A coupling agent, solid stearyl titanate, was supplied by Borica, Taiwan. The particulate carbon fiber without sizing, Tenax HT (diameter 7 µm, fiber length 60 µm and density 1.82 g/cm^3) was purchased from Teijin, USA.

The binding matrix formulation was prepared in the Brabender twin screw extruder 20/40 D and the material loading was done via gravimetric dosing units. The 6 heating zones temperature was maintained between 260 - 235 °C. The melt mixing was carried out at 375 rpm while the melt temperature was maintained between 250 – 255 °C. Initially, PA6 (73.5 wt. %) and coupling agent (1.5 wt. %) were mixed in the melting zone and followed by the addition of PCF (25 wt. %) in the mixing zone (PA6.CF). The homogenized composite material was then granulated with help of underwater granulation system. The initial material characterization was carried out by using injection molded standard specimen. The test method and the results are tabulated in Table 1.

The filament extrusion was carried out in Brabender conical twin-screw extruder Mark III and the material feeding was done via gravimetric dosing unit. The 6 heating zones were operationalized between 260 - 240 °C, while the melt temperature was between 245 – 250 °C. The extrusion speed was regulated by the melt pump, while the filament extrusion rate was maintained at 20 cm^3/min. The extruded filament was passed through an air-cooled haul off system to maintain the winding temperature near to atmospheric temperature. Meanwhile, the fiber diameter was constantly monitored with the help of BETA LaserMike ovality measurement device along with AccuNet, supplied by NDC GmbH, Germany. As shown in Figure 2, the diameter of the neat PA6 shows larger variation compared to PA6 reinforced with PCF (PA6.CF).

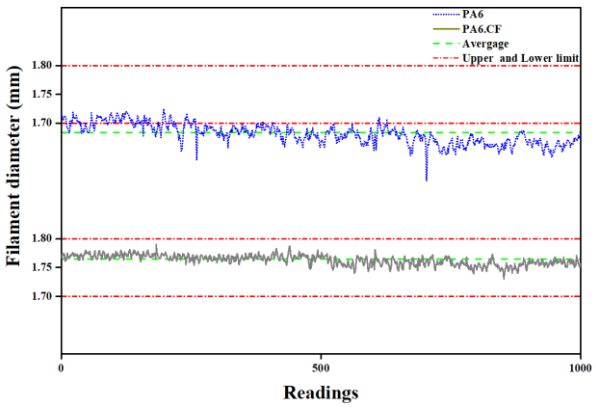

Figure 2 Measured diameter data of 1000 scans for both PA6 and PA6.CF filaments

Table 1 Material properties of injection molded specimens; mechanical properties are reported at 95% CI.

Properties	Test method	PA6	PA6.CF
Melting temperature. (°C)	ISO 11357-3	220 - 225	220 - 222
Density, (g/cm^3)	ISO 1183-1	1.130	1.190
Flexural modulus, (MPa)	ISO 178	1586 ± 23	5837 ± 138
Flexural strength, (MPa) at 3.5%	ISO 178	71.91 ± 2.80	136.8 ± 1.02
Tensile modulus, (MPa)	ISO 527-1	2630 ± 264	7427 ± 274
Tensile strength, (MPa)	ISO 527-1	63.06 ± 0.80	96.02 ± 1.90
HDT-A, (°C; 1.8 MPa – 120°C/hrs)	ISO 75-1	48 - 49	162 - 166
Charpy impact strength (notched, kJ/m^2)	ISO 179-1/eA	3.68 ± 0.39	5.90 ± 0.64

Composite flexural specimens were fabricated in Anisoprint's composer A4 series CFC printer. The standard specimen's dimension, 80 x 13 x 4 mm (L x W x H), were printed according to in-house standard. The span length of 64 mm and the testing speed of 1 mm/min were set according to internal protocol. The test was carried out with universal testing machine MESSPHYSIK BETA 50, with 5 kN load cells. The specimen's print settings (Table **2**) are defined within the AURA slicer software that prepares 3D models for manufacturing parts using composer CFC-printer as well as conventional FFF-printers. In Figure 3, the color code symbolizes different functions and materials data input; orange color represents the printing of CCF fibers with binding TP matrix (reinforced perimeter and fiber infill) via CFC print head. The black (perimeter) and light green (infill) color represent stand-alone TP printing performed via conventional FFF nozzle. The top and bottom plastic layers are disabled on purpose to increase the effective fiber volume. Furthermore, neat PA6 and PA6.CF used in this research work has the tendency to warp, which induces layer de-binding from a heated glass bed. To overcome this process disparity a high-temperature glue from vision miner, USA was applied onto glass printing bed to improve the printed part's bed adhesion. A total of 5 specimens for each material were printed and tested. The test result's error was evaluated to the significance level of 5%. Cryo-fractured fiber specimens were subjected to scanning electron micrograph (SEM). The Phenom ProX desktop SEM was utilized to study the fractured surface morphology using a secondary electron at 15 kV.

In order to quantify the defect volume and porosity percentage, the specimens were subjected to µ-CT by the laboratory CT device Nanotom 180NF (GE phoenix x-ray, Germany). The two test samples were scanned at once with a voxel size of $(4.5\ \mu m)^3$ and subsequently analyzed with the porosity/inclusion analysis tool by VGstudio MAX 3.3 (Volume Graphics GmbH, Germany). The defect and porosity analysis are based on the gray value distribution, as threshold ISO-40 (grey value at 40% between background and material peak) was used. This procedure and also different threshold methods are presented in the publication of Plank et al. [15].

Figure 3 Graphical representation of part configuration generated via slicing software AURA

Table 2 Important printing settings

Parameters	Values
CFC Nozzle temperature (°C)	240
FFF Nozzle temperature (°C)	250
CFC TP flow multiplier	1.05
CFC layer height (mm)	0.36
CFC extrusion width (mm)	0.75
FFF TP flow multiplier	1
FFF layer height (mm)	0.12
FFF extrusion width co-efficient	1.1
Bed temperature (°C)	95
TP perimeter count	2
Inner fiber perimeter count	1
Fiber infill pattern	Solid
Fiber infill angle	0
FFF print speed (mm/s)	60
CFC print speed (mm/s)	10

Results and discussion

Flexural properties

Figure 4 represents the flexural modulus and strength of the 3D printed composite specimens. The influence of coupled PCF's reinforcement on PA6 as a binding matrix (PA6.CF+CCF) is evident with approx. 46% increase in composite flexural stiffness (E_f = 20.01 ± 1.61 GPa) and approx. 27% increase in flexural strength (σ_s = 195.3 ± 17.84 MPa) when compared to neat PA6 composite (E_f = 13.72 ± 1.08 GPa, σ_s = 153.1 ± 5.923 MPa). Likewise, Peng et al. [5] reported that increase in average fiber volume increased the tensile strength of the CFRTP composites, specifically in short carbon fiber (SCF) reinforced polyamide matrix. Furthermore, the authors

also noted that the SCF reinforcement had no influence on elastic modulus and inferred this phenomenon as the out of plane orientation of SCF in the top and bottom TP layers (infill orientation ±45°). However, Adumitroaie et al. [8] reported the decrease in average fiber volume content, about 25-27% in 3D CFC printed parts compared to approx. 60% average fiber volume in CCF. Incidentally, the loss of average fiber volume is clearly recouped by PCF in TP matrix, especially for the transversal loading application where the surplus of the applied stress enduring ability is predominantly realized by TP's matrix. Furthermore, micro CT scans reveal higher defect volume for PA6+CCF and PA6.CF+CCF (see Table 3). Henceforth, the phenomenon is an indication that both TP filaments (neat and reinforced) need further process optimization and subsequent process validation.

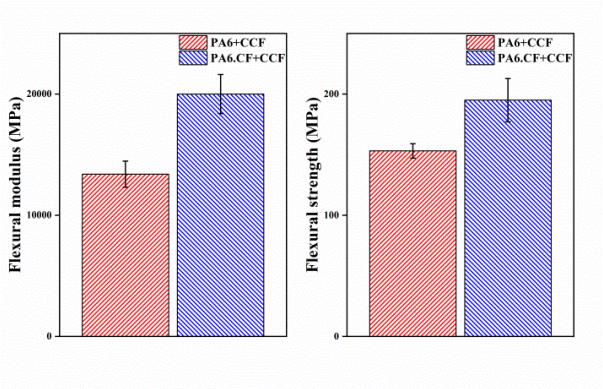

Figure 4 Flexural modulus and flexural strength results obtained via three-point bending test

Morphology

The SEM micrographs of the cryo-fracture surface of the thermoset carbon fiber composite, CCF and injection molded impact tested specimen are shown in Figure 5 (a) and Figure 5 (b), respectively. Initial inference from the SEM images of CCF showed a large number of carbon fiber breakages, and impeccable distribution of carbon fibers indicate optimal curing conditions are satisfied. On the contrary, few fibers pull out can be clearly distinguished from the evenly distributed fiber cluster and this phenomenon can be attributed to sampling preparation. Cryo-fracturing of the composite fiber involves bending and its significance is clearly visible, the fiber pull out is due to tension being applied (bending) on side of the fiber, whereas compression is assumed to be predominant on the opposite section (fiber breakage). Furthermore, the impact tested PA6.CF specimens show brittle fracture and fiber pull-out. And the foremost aspect of the impact fracture surface is the fiber alignment and enhanced matrix-fiber compatibility (no visible fiber slippage). Similar to Spoerk et al. [13], Jiang and Smith [14] report, the fibers have oriented in the flow direction (in-plane), and this will result in highly anisotropic behavior in 3D printed parts.

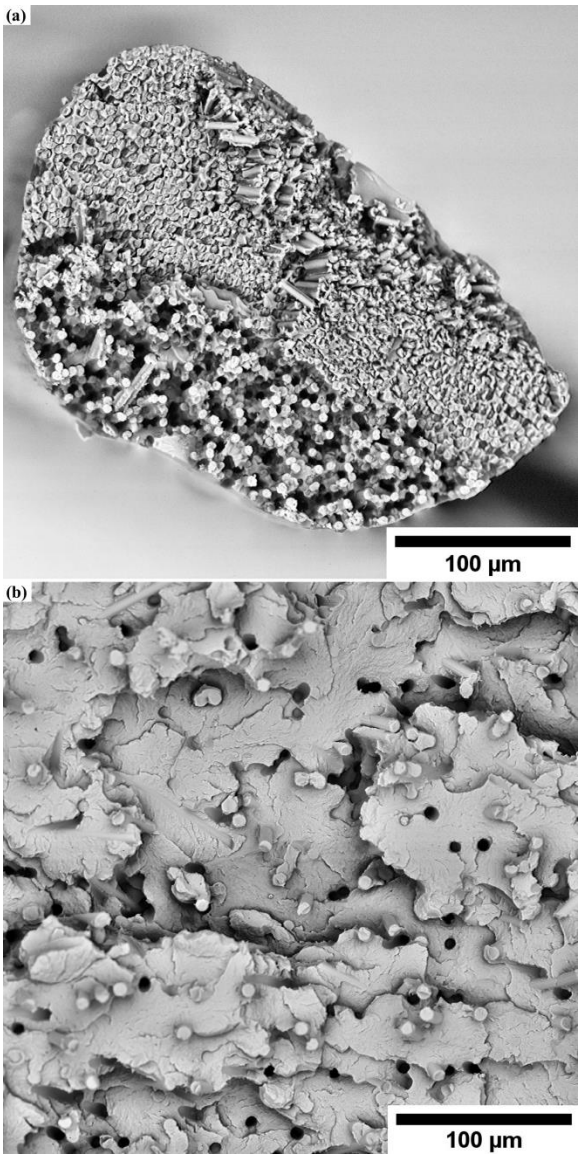

Figure 5 SEM images of cryo-fractured composite fibers, CCF from Anisoprint (a) and impact tested PA6.CF (b).

The defect-free process for preparing uni- and multi-directional composites is achieved via precise control, temperature and maintaining void content well below 1%. The cross-sectional µ-CT images showed clear distinct segregation between voids and TP matrices. In Figure 6 the results of the porosity analysis are shown exemplarily for cross-sectional images in the ZY-plane. The cyan line around the sample in Figure 6 defines the region of interest (ROI) for which the porosity analysis was carried out. Voids and porosities are color-coded according to the scale bars and reveal the differences in the porosities. Furthermore, both samples have sizeable voids, the PA6.CF+CCF has a large void in the range of 45 to 55 mm^3 (red) but also small voids up to 15 mm^3 (blue),

whereas the voids in the PA6+CCF sample have varying sizes and clearly makeup to 20 mm^3. The results of the µ-CT help in identifying and quantifying the defects that are visually indistinguishable and subsequently calibrate the printing process setting to achieve void content below 1%. Table 3 shows the determined total volume and defect volume and subsequent calculation of porosity percentage emphasizes the colored images. The porosities of the PA6+CCF and PA6.CF+CCF have the same quantity of porosity.

A higher ISO threshold value would avoid under segmentation of the big voids, which appear in Figure 6 as unsegmented small spots in bigger voids. By using a higher ISO threshold also those areas would be segmented, but contrary it leads to the segmentation of areas with similar gray values which might be artifacts, but cannot be verified due to the limited resolution. Additional high-resolution scans (with smaller sample size) could be used for the enhancement of the threshold value [14, 15]. Moreover, the results of the porosity analysis can be compared due to the fact that they were scanned at once and undergo the same segmentation and analysis procedure.

Table 3 Porosity and defects determined by µ-CT with ISO 40 threshold

Specimen	Total volume (mm^3)	Defect volume (mm^3)	Porosity (%)
PA6+CCF	347.7	58.5	16.8
PA6.CF+CCF	355.2	59.1	16.6

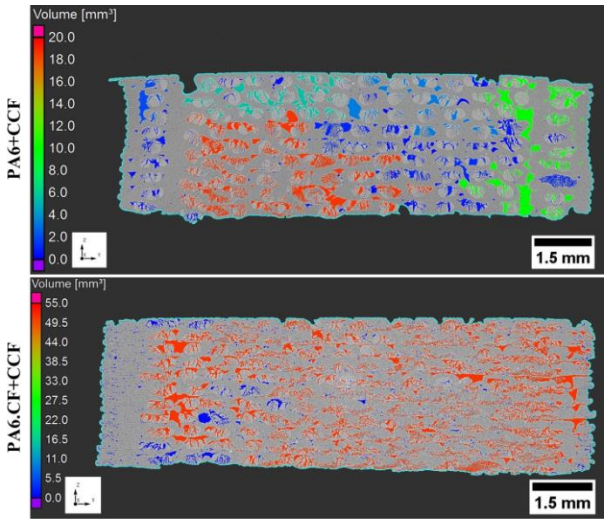

Figure 6 Measured cross-sectional µ-CT scan images of composite parts along with respective defective volume scalar intensity bar.

Conclusion

In summary, compared to neat PA6, the PCF reinforced PA6 binding matrix exhibited overall positive influence on the composite specimen fabricated in CFC 3D printer. Furthermore, the loss of average fiber volume in CFC specimens is evidently compensated with reinforcing PCF. The fractography of CCF fiber revealed defect-free and high compatibility between thermoset matrix and carbon fibers. Similarly, the stearyl titanate coupling agent has improved the compatibility between PA6 matrix and particulate carbon fibers. The µ-CT scan revealed that large internal defects may have contributed to the loss of mechanical properties indicating optimal printing conditions are not accomplished.

The future investigations will be mainly focused on factors such as printing settings and process optimization for different binding TP's matrices in CFC technology

Acknowledgment

This research work has been performed as part of the "3D-CFRP" project. The authors acknowledge the financial support by the EU funded network M-Era.Net, the BMVIT (Austrian Ministry for Transport, Innovation, and Technology), the FFG (Austrian Research Promotion Agency), as well as the RCL (Research Council of Lithuania) and FASIE (Foundation for Assistance to Small Innovative Enterprises, Russia). Authors express gratitude to Konrad Wipplinger, Oliver Katzenberger, and Romana Welser of Kompetentzzentrum Holz GmbH for the sample preparation.

References

1. X. Tian, T. Liu, C. Yang, Q. Wang, and D. Li, *Composites Part A: Applied Science and Manufacturing*, 88, 198 (2016).
2. N. Li, Y. Li, and S. Liu, *Journal of Materials Processing Technology*, *238*, 218 (2016)
3. L. Meng, T. Xiaoyong, S. Jungan, Z. Weijun, L. Dichen, and Q. Yingjie, *Composites Part A*, 121, 130 (2019)
4. N. Van de Werken, J. Hurley, P. Khanbolouki, A. N. Sarvestani, and A. Y. Tamijani, *Composites Part B*, 160, 684 (2019)
5. Y. Peng, Y. Wu, K. Wang, G. Gao, and S. Azhi, *Composites Structures*, 207, 232 (2019)
6. M. Eichenhofer, J. C. H. Wong, and P. Ermanni, *Additive Manufacturing*, 18, 48 (2017)
7. A. V Azarov, F. K. Antonov, M. V. Golubev, and A. R. Khaziev, *Composites Part B*, 169, 157 (2019)
8. A. Adumitroaie, F. Antonov, A. Khaziev, A. Azarov, M. Golubev, and V. V. Vasiliev, *Materials*, 12, 3011 (2019)
9. H. Albrecht, C. Savandaiah, A. Lepschi, B. L. Baselli, and A. Haider, *Proceedings in II*

international conference on Simulation for Additive Manufacturing, 147 (2019)
10. V. A. Andrey, V. V. Valery, F. R. Alexandr, and A S. Vladimir, EU patent, EP3450486A1 (2019).
11. M. Spoerk, C. Savandaiah, F. Arbeiter, S. Schuschnigg, and C. Holzer, *SPE-ANTEC-Anaheim*, 105 (2017).
12. M. Spoerk, C. Savandaiah, F. Arbeiter, J. Sapkota, and C. Holzer, *Polymer Composites*, 83, 768 (2017)
13. M. Spoerk, C. Savandaiah, F. Arbeiter, G. Traxler, L. Cardon, C. Holzer, and J. Sapkota, *Composites Part A*, 113, 95 (2018)
14. D. Jiang, D. E. Smith, *Additive manufacturing*, 18, 84 (2017)
15. B. Plank, G. Rao, and J. Kastner, *Proceedings in 7th International Symposium on NDT in Aerospace*, 10 (2015)
16. B. Plank, C. Gusenbauer, S. Senck, H. Hoeller, and J. kastner, *Proceedings in 12th European conference on Non-destructive Testing*, 1, (2018)